International Journal of Biological Macromolecules 209 (2022) 1562–1572

Contents lists available at ScienceDirect

International Journal of Biological Macromolecules

journal homepage: www.elsevier.com/locate/ijbiomac

Colorimetric food spoilage monitoring with carbon dot and UV light reinforced fish gelatin films using a smartphone application

Beyza Kilic [a], Vakkas Dogan [b], Volkan Kilic [b], Leyla Nesrin Kahyaoglu [a,*]

[a] Department of Food Engineering, Middle East Technical University, 06800 Ankara, Turkey
[b] Department of Electrical and Electronics Engineering, Izmir Katip Celebi University, 35620 Izmir, Turkey

ARTICLE INFO

Keywords:
Carbon dot
UV irradiation
Fish gelatin
Colorimetric detection
Smartphone application

ABSTRACT

The objective of this study was to develop novel colorimetric films for food freshness monitoring. UV light irradiation (365 nm) and carbon dots (CDs) were tested as the potential crosslinkers in the fabrication of anthocyanins doped fish gelatin (FG) films. The effect of crosslinkers on the optical, surface, structural, barrier and mechanical properties of FG films was investigated. The incorporation of CDs under UV irradiation improved the tested properties of FG films. The kinetic colorimetric responses of FG films against ammonia vapor were studied to simulate the food spoilage and determine the ammonia sensitivity of the films. Among the tested films, UV-treated FG films containing 100 mg/l (FG-UV-CD100) indicated the best properties. Later, the color difference of FG-UV-CD100 films was observed to correlate well with microbial growth and TVB-N release in skinless chicken breast samples. At the same time, a custom-designed smartphone application (*SmartFood*) was developed to be used with the FG-UV-CD100 film for quantitative estimation of food freshness in real-time. The proposed food freshness monitoring platform reveals a great potential to minimize global food waste and the outbreak of foodborne illness.

1. Introduction

Consumers often evaluate food freshness using estimated expiration dates on traditional food packages. However, date labels create widespread confusion among consumers and promote food waste globally [1]. Consumers tend to throw away food products due to perceived safety and quality concerns even when the date on the label is close but not past the expiration date [2]. Unfortunately, general consumer behavior regarding date label perception contributes to an estimated global food waste of about 1.3 billion tonnes per year, according to the Food and Agriculture Organization. Therefore, if one could fabricate a low-cost platform that could provide real-time information on food quality/freshness, it would be a great advancement in both protection of consumers against potential foodborne illness and prevention of global food waste. In this context, smart packaging offers an excellent alternative to the concept of expiration date label with the aforementioned shortcomings as it aims to monitor and display the freshness of food until consumption.

So far, three main types of smart tools commercially used in food packaging systems have been developed: barcodes, sensors and displays [3]. Sensors and barcodes usually require expensive components, which make them more suitable for the pharmaceutical industry rather than the food. For a food product, the packaging cost should be less than 10% of the total cost of the food item to stay within a reasonable profit margin [4]. Thus, comparably inexpensive pH-responsive pigments and dyes are widely used as freshness indicators, which provide user-friendly visual information through color change when food spoils [5]. Among these natural dyes and pigments, anthocyanins exhibit visible color changes in response to a wide pH range. To date, anthocyanins have been immobilized by entrapment into different biodegradable polymers, including but not limited to cellulose, chitosan, and gelatin [6]. Gelatin is a water-soluble biopolymer obtained from the irreversible hydrolysis of collagen, the most abundant protein in animals. Cattle hides, bones, and pigskin are primarily used in gelatin production [7]. On the other hand, fish gelatin (FG) shows no risk of Bovine Spongiform Encephalopathy and has the Kosher and Halal status that meets the demand of specific religious groups compared to its counterparts [8]. Additionally, FG films have lower water vapor permeability (WVP) than their counterparts [9], making FG particularly useful in food packaging applications. Despite the above advantages, a major bottleneck in the widespread use of FG for composite film applications is its low melting point. Thus, chemical and physical methods have been used to reinforce the FG film structure.

* Corresponding author.
E-mail address: kaleyla@metu.edu.tr (L.N. Kahyaoglu).

https://doi.org/10.1016/j.ijbiomac.2022.04.119
Received 7 February 2022; Received in revised form 12 April 2022; Accepted 17 April 2022
Available online 22 April 2022

In the last decade, natural chemical crosslinkers including sugars [10,11], organic acids [12], phenolics [13] have been widely studied for this purpose.

In addition to natural crosslinkers, a cheap, facile and eco-friendly physical method, radiation induced crosslinking has gained interest [14]. Among the different types of electromagnetic radiation, the nondestructive effect of ultraviolet (UV) radiation was reported to be a promising approach for mechanical improvements of FG films [7,15]. UV radiation induces radical formation at the aromatic amino acid residues of gelatin, which leads to crosslinking and, thereby mechanical improvement of the film structure [7]. Other than the listed crosslinkers, nanoparticles with surface functional groups might be incorporated into the FG matrix to fabricate a mechanically enhanced nanocomposite structure. In this sense, carbon dots (CDs) synthesized from carbon sources might be good candidates with abundant surface functional groups [16]. Moreover, CDs outperform other nanomaterials in terms of facile synthesis from cheap precursors, photoluminesce yield and toxicity [17]. Here, carboxyl-functionalized CDs were used to develop a novel FG-based nanocomposite film under UV irradiation without using any toxic crosslinkers.

Colorimetric sensing provides direct visual inspection for qualitative and quantitative analysis of molecular interactions without complex tools, driven by applications such as pregnancy, urine and pH test strips where discoloration in the sensing zone leads to an outcome [18–20]. However, it might still be challenging for consumers to determine the freshness of food by visual inspection alone due to the limitations of the human eye in perceiving color intensity change in the case of less pronounced color transition [21,22]. Therefore, capturing the color change with a camera and measuring the color intensity under imaging software can provide the necessary data for quantitative analysis [23–25]. The latest technological advances in cameras and sensors enable smartphones to be built with powerful processors and high resolution digital cameras, providing fast and reliable colorimetric analysis with custom-designed smartphone apps. In this regard, integrating a smartphone as an image capturing and processing device into the sensing module can minimize consumer misconceptions caused by the expiry date labels. To estimate the freshness and quality of food, colorimetric film images captured by a smartphone camera can be processed using a custom-designed mobile app. Using this application on a ubiquitous smartphone allows consumers to monitor food conditions easily and minimize the risk of food poisoning and food waste. The main objective of this study was to develop a simple yet powerful colorimetric sensing scheme compatible with smartphone technology based on anthocyanins doped FG films reinforced with CD and UV light. Sensor films at different CD concentrations were characterized in terms of mechanical, thermal and structural properties. Then, the color response of the FG films against ammonia vapor was systematically studied to develop a mobile application named *SmartFood*. Food spoilage was successfully monitored through the color change of the developed film with the *SmartFood* app.

2. Material and methods

2.1. Materials

FG (200 bloom) was supplied kindly by SG Chemicals. Sodium phosphate monobasic and potassium phosphate dibasic, magnesium oxide, boric acid, and bromocresol green-methyl red mixed indicator solution were purchased from Sigma-Aldrich (St. Louis, MO). Hydrochloric acid fuming (37%) and ammonium chloride, citric acid were purchased from ISOLAB (Wertheim, Germany). Ammonium hydroxide solution (32%) was provided by Merck (Darmstadt, Germany).

2.2. Fabrication of colorimetric films

2.2.1. Red cabbage anthocyanins (RCA) extraction

Anthocyanins were extracted from red cabbage according to the method described by Chandrasekhar et al. [26]. A sample of 50 g of red cabbage was cut into small pieces with a chopper and macerated in 100 ml of distilled water by stirring for 24 h at 450 rpm. Next, the extract was filtered first through Whatman paper #1 and then 0.45 μm syringe filter. RCA concentration was estimated with the help of the pH differential method [27]. Stock RCA concentration was adjusted to 1 mg/l in 100 mM sodium phosphate buffer at pH 6 and stored in the dark at 4 °C until further use.

2.2.2. Synthesis of carbon dots

Carboxyl-functionalized CDs were synthesized through carbonization of citric acid by a microwave-assisted method described by Dhenadhayalan method [16]. Briefly, 10% *w/v* citric acid solution was prepared in distilled water and heated at 550 W for 7 min in a microwave lab station (Ethos D Microwave Labstation, Milestone Inc., USA). The solution color turned to brownish yellow from colorless after microwave heat treatment. The obtained foamy residue was dissolved in distilled water and dialyzed against ultrapure water with a dialysis tubing (1200 Da cutoff, Sigma, D7884–10 FT) for 48 h. Subsequently, the synthesized CD was freeze-dried (Christ Alpha 2–4 LD Plus, Martin Christ, Ger- many) for characterization and experimental purposes. For film fabrication, 1 g/ml stock CD solution was prepared in 100 mM sodium phosphate buffer at pH 8.

2.2.3. Spectral analysis of RCA and CDs

UV–Vis spectra of RCA and CD solutions were measured using a UV–Vis spectrophotometer (Optizen Pop, Mecasys, Seoul, Korea). The spectra were determined in 100 mM sodium phosphate buffers with a pH range of 1.0–12.0 between 400–680 nm for RCA solutions while the spectral measurements were performed in 100 mM sodium phosphate buffers with a pH range of 2.0–12.0 between 300 and 460 nm for CD solutions.

2.2.4. Fabrication of fish gelatin films

The FG films were fabricated through the solvent casting method by mixing FG, RCA, glycerol and CD. Final concentrations of FG, RCA and glycerol were kept in all precursor solutions constant at 10% *w/v*, 0.5 mg/l and 1% w/v, respectively. First, FG was dissolved in 100 mM sodium phosphate buffer at pH 8 and stirred at 50 °C until a clear solution was obtained. Then, RCA was added from the stock solution. Similarly, CD from stock solution was incorporated into the precursor solution at this stage for CD containing samples. Subsequently, glycerol was added as a plasticizer, and the pH of the solution was adjusted to 8. The precursor solution was ultrasonicated for 45 min at 50 °C. Two different approaches were followed after the precursor solution was obtained. In the first approach, 15 ml of the solution was poured into a polystyrene Petri dish (9 cm in diameter) and directly placed into the desiccator with silica gel (0% relative humidity) at 23 °C for 48 h. This control sample was marked as FG. In the second approach, the precursor solution in the Petri dish was irradiated with UV light (1.5 mW/cm, 365 nm, Vilber ECX-F20.L-V1) for 45 min before placing into the desiccator. This control sample was designated as FG-UV. Samples with varying concentrations of CDs (25 mg/l, 50 mg/l and 100 mg/l) were prepared following the second approach described above and as FG-UV-CD25, FG-UV-CD50 and FG-UV-CD100. The desiccators used in the experiments were levelled with a spirit air bubble level before placing the precursor film solutions. All films were conditioned at 25 °C and relative humidity (RH) of 52% before analysis in a climate chamber (TK120, Nuve, Ankara, Turkey).

2.3. Characterization of colorimetric films

2.3.1. Mechanical and barrier properties of the films

The mechanical properties of the films were determined using a Zwick/Roell Z250 universal testing machine (Ulm, Germany). For mechanical tests, films were casted onto a 12 × 12 cm square petri dishes

using the procedure described in Section 2.2.4. Prior to tensile testing, the films were cut into a dog bone shape (a gauge length of 25 mm and the width of 4 mm) with a manual cutting press (ZCP 020, Zwick GmbH&Co., Ulm, Germany). Mechanical tests were performed in an environment conditioned at 51 ± 1% relative humidity and at a temperature of 24 ± 1 °C with a Tecnair LV climatic room conditioner. The samples were mounted between the pneumatic grips with initial separation of 20 mm and then pulled apart at cross-head speed of 50 mm/min. For each film type, three samples were tested. TS and EAB values of each sample were calculated using the testXpert testing software. Tensile strength was measured as the ratio of maximum load before the rupture to cross sectional area of the films. Percentage elongation at break was calculated as the ratio of the increase in length till the rupture of films to initial length. The WVP of films was determined with the method described by McHugh et al. [28]. The thickness of the films was read at 7 different points with a digital micrometer (LOYKA 5202–25, Loyka, Ankara, Turkey). The cylindrical test cup with an internal diameter of 4 cm was filled with 35 mL water to provide 100%RH. The film sample was sandwiched between the cup and its cap. The initial weights of the cups were recorded. Then, the cups were placed into a silica gel-filled desiccator. The temperature and relative humidity change inside the desiccator and the weight changes of the cups were recorded for 12 h at 1 h intervals. WVP was calculated as g/m.s.Pa [28].

2.3.2. Moisture content and water solubility of the films

For moisture content measurements, the films were cut into pieces (2 cm × 2 cm) and weighted (W_0). The films were then dried at 105 °C until the constant weight (W_1) was attained. Percent moisture content (%MC) was determined by Eq. (1).

$$\%MC = \frac{W_0 - W_1}{W_1} \times 100 \quad (1)$$

The water solubility of films was determined with minor modifications from the method described by Gontard et al. [29]. Briefly, the 2 cm × 2 cm pieces were immersed in 50 mL distilled water for 24 h at room temperature. Excess water was removed by the filter paper after removal, and the films were dried at 105 °C until constant final weights (W_2) were reached. Water solubility (WS) was calculated by Eq. (2).

$$WS = \frac{W_0\left(1 - \frac{\%MC}{100}\right) - W_2}{W_0\left(1 - \frac{\%MC}{100}\right) - W_2}\, x\ 100 \quad (2)$$

2.3.3. Thermal properties of the films

Thermal properties of films were determined by differential scanning calorimeter (Perkin Elmer, DSC 4000, CT, USA). After the film samples were dried in a vacuum oven at 40 °C for 48 h, each sample was weighed into aluminum pans (5 mg) and sealed. Scanning was carried out under inert nitrogen gas in the range of −20 to 120 °C with a heating rate of 10 °C/min. The empty sealed pan was taken as a reference during the scanning.

2.3.4. Structural analysis

The morphology of the CDs was determined by a high resolution transmission electron microscope (HRTEM) (FEI, Tecnai G2 Spirit Biotwin, Oregon, USA) under an accelerated voltage of 20–120 kV. The cross sectional morphologies of the films were observed with the Scanning Electron Microscope (FESEM) (FEI, QUANTA 400F Field Emission SEM, Oregon, USA) with 5 kV accelerating voltage. All film samples were cryofractured. The chemical bond interactions and changes were examined by the attenuated total reflection Fourier transform infrared spectroscopy (ATR-FTIR) (SHIMADZU, IRSpirit, Kyoto, Japan). FTIR spectra of CD, RCA and the films were measured in the range of 4000–750 cm^{-1} at 4 cm^{-1} resolution in transmission mode. The crystallinity was investigated with an X-Ray diffractometer (XRD) (Rigaku, MiniFlex XRD, Tokyo, Japan) over 2θ in the10° to70° range for CD and in the 5° to 55° range for FG films. Films were conditioned at 50% relative humidity before experimentation and CDs were freeze-dried. Percent relative crystallinity was estimated by Eq. (3).

$$X_c = \frac{A_c}{A_c + A_a}\, x100 \quad (3)$$

where A_a and A_c are the diffraction peak area of the amorphous region and crystalline phase calculated from diffraction patterns, respectively.

2.3.5. Colorimetric response of the films to volatile ammonia

Color response of the films to volatile ammonia was monitored using absorbance measurements [30]. Changes of absorbance upon exposure to ammonia vapor were determined by placing the colorimetric films (2 cm × 2 cm) at 1 cm above the ammonia solution (0.8 M, 20 ml) for 16 min at 23 °C. The absorbance ratio of the films at 605 nm versus 530 nm (A605/A530) was recorded every 1 min spectrophotometrically (Multiskan Sky, Thermo Scientific, Tokyo, Japan). The color response of the films was tested against different concentrations of ammonia gas by placing (2 cm × 2 cm) film pieces above the ammonia solution in beakers (25 ml). For this purpose, the stock solution of ammonium chloride (1 M) and sodium hydroxide (0.2 M) were prepared. The concentration of gaseous ammonia was calculated using its initial concentration in 20 mL solution and the partial vapor pressure of ammonia at 23 °C using Raoult's law [31]. The beaker was sealed after a calculated amount of stock solutions was injected to generate in situ ammonia gas concentration corresponding to 5, 10, 20, 30, 60, 90 and 120 mg N/100 g at 23 °C. Water was used as a reference solution for 0 mg N/100 g. Images of the films were taken after 6 h of exposure to ammonia solutions at 23 °C image capturing details in Section 2.4. The values of L* were lightness, a* was the red to green, and b* was the yellow to blue. The values of L*, a*, b* were extracted from the captured images with the ImageJ program to calculate the value of color difference index ΔE (Eq. (4)).

$$\Delta E = \sqrt{\left(L_0^* - L^*\right)^2 + \left(a_0^* - a^*\right)^2 + \left(b_0^* - b\right)^2} \quad (4)$$

where L^*_0, a^*_0, and b^*_0 are the values of the reference sample exposed to water and L, a, and b are the values after exposure to different concentrations of ammonia vapor.

2.3.6. Chicken spoilage trials

10 g of skinless chicken breast was prepared aseptically and placed to the bottom of UV light sterilized (254 nm, 15 min) polystyrene foam cups with 5 cm height. Small squares (2 cm × 2 cm) of colorimetric films were fixed on cellophane and sealed 1 cm above the chicken samples. The cups were stored at 4 °C for 9 days of the trial. The color change of the films was recorded with the smartphone (LG, G6, Yeouido-dong, Seoul, South Korea) and evaluated every 24 h with the smartphone application developed in this study.

2.3.7. TVB-N measurements

10 g of skinless chicken breast was homogenized for 2 min in 100 ml sterile distilled water in the stomacher (Wisd, WES-400 model) [32]. The homogenate was centrifugated for 12 min at 10000 rpm. The supernatant was collected and mixed with an equal volume of magnesium oxide solution (1% *w/v*). Steam distillation was carried out by collecting the distillate in a flask containing 25 ml of boric acid (20 g/l) and a few drops of methyl red/bromocrosol green indicator. After the distillation, the final mixture was titrated with 0.01 M HCl until the blue color turned pink. The TVB-N of the sample was calculated by Eq. 5.

$$\text{TVB} - \text{N (mg/100 g sample)} = \frac{(V_1 - V_0).0.14.1.100}{M} \quad (5)$$

where V_1 (mL) is the volume of 0.01 M HCl solution for sample, V_0 (mL) is the volume of 0.01 M HCl solution for blank and M(g) is the weight of the sample.

2.3.8. Microbial analysis

Skinless chicken breast samples were tested for the levels of total viable aerobic bacteria. 10 g of chicken breast and 100 mL of sterile peptone water were put into the sterile stomacher bag and homogenized at stomacher (Wisd, WES- 400 model) for 2 min. A series of decimal dilutions were performed with respect to recommend microbiological protocols [33]. 1 mL of each appropriate dilution was pour plated on Plate Count Agar and incubated aerobically at 30 °C for 48 h. The number of colony-forming units (cfu) was counted and reported as log cfu/g.

2.3.9. Statistical analysis

All experiments were conducted in triplicate. Data were analyzed using the statistical analysis software (OriginPro) with Tukey's posthoc test. Statistical significance was defined for the differences where the *p*-value was less than 5% ($p < 0.05$).

2.4. Experimental design and image capturing

The mobile platform for colorimetric food monitoring was manufactured to attach with LG G6 (1/3.06 inch sensor size, 1440 × 2880 resolution, 1.12 μm pixel width) to take advantage of the rear-facing camera and flash for image capturing. The smartphone flash offers illumination stability in capturing, leading to a consistent intensity variation between successive concentration changes. Our custom-designed cradle was fabricated with a smartphone case holder using a 3D printer, as illustrated in Figure S1, which provides a con- trolled environment regardless of ambient light conditions. Images were captured in manual mode with the same camera (1/320 s, 100 and f1.8 for shutter speed, ISO and focus levels, respectively) and white balance settings to en- sure consistency and repeatability. The images were then transferred to a computer for further processing in MATLAB (MathWorks, MA, USA). Air bubbles or light reflections in colorimetric films (first row in Figure S2) can degrade colorimetric analysis, so a resizable box was used for manual determination of the region of interest (ROI). The ROI of samples for different concentrations is given in the second row of Figure S2, used to derive the calibration curve for the colorimetric analysis. Several color features, including mean, skewness and kurtosis, were calculated for 9 different channels (R, G, B, H, S, V, L*, a*, b*) to find the best calibration curve representing the characteristic of intensity variation with respect to the concentration change. In this regard, the RGB image was converted to HSV and L*a*b* (Lightness, Green-Red, Blue-Yellow) color channels. Besides the color features, texture features such as contrast, correlation, homogeneity, and energy were also calculated. Furthermore, 33 features with entropy and intensity were examined to obtain the calibration curve with the highest R^2 value, which was later integrated into our smartphone application called *SmartFood*.

2.5. Smartphone application: ***SmartFood***

Our custom-designed Android application, *SmartFood*, was developed for colorimetric food monitoring and spoilage detection, capable of performing colorimetric analysis without an internet connection (offline). The calibration curve described in the previous subsection was formulated to be coded in Android Studio, which offers rapid on-site quantitative monitoring. As the calibration curve is embedded in the application, no internet connection is required to transfer and process the data. Under the simple, user-friendly interface of the application (Fig. 6), non-expert users can efficiently perform image operations such as viewing and cropping. The homepage is shown in Fig. 6a, where the user can select the image from the gallery or take a new image using the camera. The selection of the ROI with an adjustable crop box is illustrated in Fig. 6b-c-e-f. When the "COMPUTE" button is tapped in Fig. 6c and f, the concentration value is calculated based on the calibration curve and displayed on the screen (Fig. 6d and g).

3. Results and discussion

3.1. Optical characterization of RCA

The color change of RCA solutions is shown in the inset image of Fig. 1a over the pH range of 1 to 12. As illustrated, the color of the solutions was reddish-pink at pH values lower than 5 and turned gradually to purple at pH 6–7. When the pH values went above 7, the color changed to different shades of green between pH 8–11 and turned yellow at pH 12. The UV–Vis spectra of anthocyanins at different pH values are illustrated in Fig. 1a. At pH 5 and lower, the maximum absorption peak was observed at 520 nm and this peak decreased and gradually shifted to 610 nm between pH 1 and pH 7 due to hypochromic and bathochromic effects. Hyperchromic effect dominated from pH 7 to pH 10,resulting in a gradual increase of maximum absorption peak intensity at 610 nm and this was followed by a decrease in the intensity from pH 10–12. Colorimetric and spectral properties of RCA solutions were consistent with the findings in the literature for the extracts of red cabbage [34,35].

3.2. Optical and physical characterization of CD

The CDs exhibited a maximum light absorption peak around 360 nm, ascribed to the overlap of $\pi-\pi^*$ transitions of C═C functional groups and $\eta-\pi^*$ transitions of C═O and other oxygen-bearing functional groups [36]. The size and morphology of the CDs were investigated by HRTEM (Fig. 1c). TEM image clearly showed that the synthesized CDs were spherical in shape with an average size of 3 nm and well-dispersed. XRD is a common method to characterize and analyze the atomic arrangements and crystal structures of compounds. The diffraction pattern of CD displays typical diffraction peak at around 21°, which confirms the successful carbonization process [16] (Fig. 1d). The observed broad and weak diffraction peak of CD might be explained by the partial carbonization and amorphous nature of CD [37].

The FTIR spectrum is given in Fig. 2a, which provides information regarding the functional groups of CD. The characteristic stretching vibrations of absorption bands due to O—H stretching vibration of the carboxylic group were observed as a broad peak around 3250 cm^{-1} and 1085 cm^{-1}, respectively. C—H vibration peak appeared weakly around 2950 cm^{-1}. Th carboxylic functional group present on the surface of CD was confirmed by a peak at 1701 cm^{-1} assigned to C═O stretching vibrations of the carboxylic group [16]. Further, the peaks around 1570 cm^{-1} and 1385 cm^{-1} might be attributed to the asymmetric and symmetric stretching of −COO− groups, respectively [38]. These findings provide evidence that the surface of CDs contains carboxyl, hydroxyl and carboxylate functional groups. The FTIR analysis also validates the successful synthesis of CDs with surface carbonyl functional groups. In this study, CDs particularly with the observed surface carboxyl groups were expected to act as chemical crosslinkers by reacting with the amine groups of FG and thereby, reinforcing the fabricated FG films.

3.3. Analysis of the surface functional groups

The FTIR spectrum of RCA indicates a broad hydroxyl stretching peak at 3258 cm^{-1} with the CH stretching vibrations at 2926 cm^{-1} due to aromatic groups in Fig. 2b [39]. The stretching vibration at 2362 cm^{-1} might be attributed to −C=O+, flavylium cation of anthocyanins [39]. In addition, C=C stretching vibration peak of the benzopyran aromatic ring was observed at 1590 cm^{-1}. A peak appearing at 1396 cm^{-1} was assigned to C—O angular deformation of phenols, while pyran aromatic ring stretching vibration of flavonoid compounds is observed at 1024 cm^{-1} [40]. All FG films showed the typical bands for N—H stretching vibrations of amide A and free/bounded hydroxyl groups above 3000 cm^{-1} and for C—H stretching vibrations of amide B around 2930 cm^{-1} (Fig. 2b). Similarly, the bands around 1630, 1540 and 1235 cm^{-1} represented C═O and C—N stretching of amide I, N—H bending

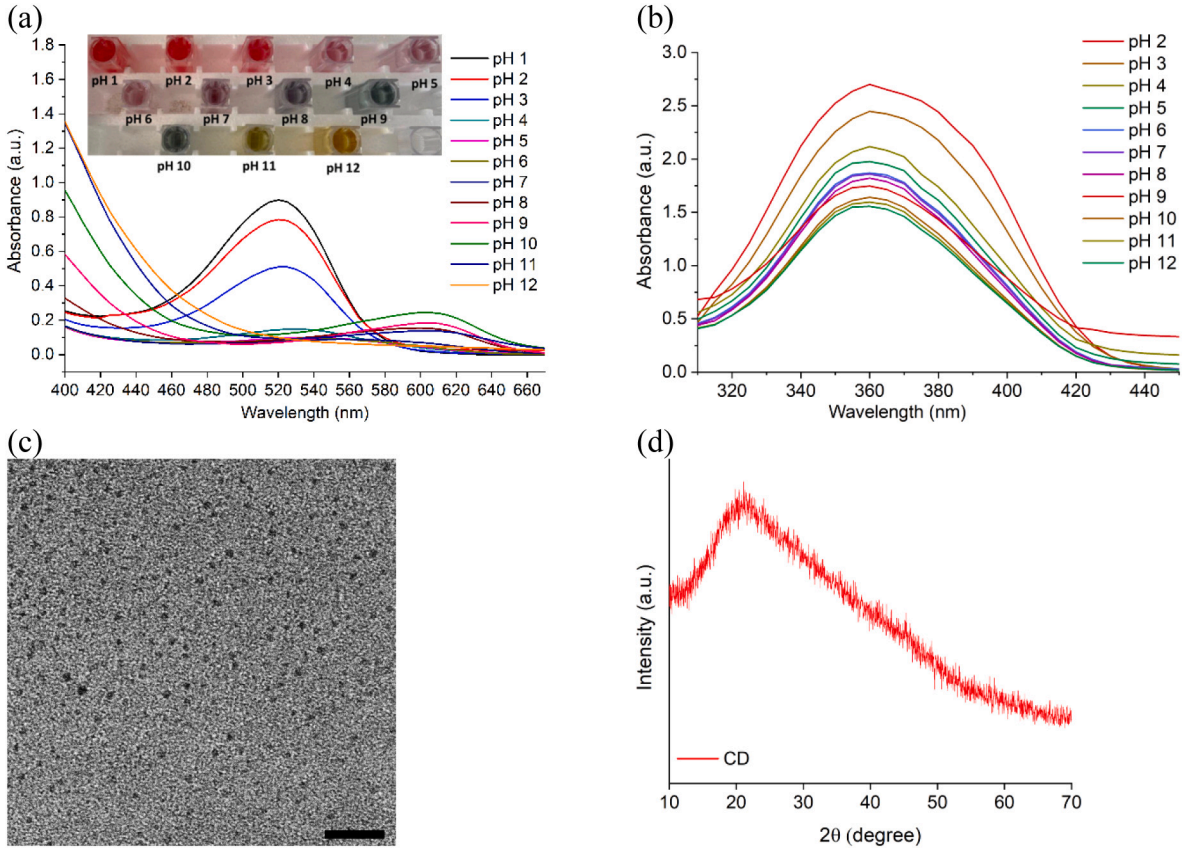

Fig. 1. UV–Vis absorption spectra of (a) RCA solutions at pH 1–12 and (b)CD solutions at pH 2–12. (c) TEM image of CDs (scale bar:20 nm) (d) XRD pattern of CDs.

and C—N stretching vibrations of amide II and the vibrations in the plane of N—H and C—N groups of amide III, respectively [41]. Even though all films showed similar spectra, the relative intensity between amide I and amide II changed gradually upon the addition of CD. The effect of CD addition was more noticeable when higher concentrations were incorporated into the film matrix. Particularly, the relative intensity of the amide I band decreased remarkably for FG-UV-CD100 film, as illustrated in Fig. 2b. Meantime, the band located around 1390 cm^{-1} was assigned to hydroxyl bending of carboxylic acid while the band appearing around 1035 cm^{-1} was attributed to the hydrogen bonding between CD, glycerol and FG. These two bands became sharp and intense upon the addition of CD at 0.1 g/L [42,43]. Similar results were also observed when citric acid and CD were incorporated into gelatin films as crosslinkers [12,43]. When CD was incorporated into FG films, the peak of CD at 1701 cm^{-1} disappeared, suggesting the possible crosslinking reaction between the carboxylic group of CD and the amine group of gelatin (Fig. 2). When these two functional groups react, theoretically, both imide and amide bond formations are possible [12]. No peak appeared around 1770 cm^{-1} on the FTIR spectrum, indicating the imide bond formation, while the amide I peak was observed at 1630 cm^{-1}. Thus, amide bond formation was considered the major crosslinking reaction in this study. Similar results were reported in the literature [12,43]. Here we promote the crosslinking reaction between the amine groups of gelatin and the carboxylic groups of CD by preparing the precursor solution of FG films under basic conditions, which is expected to induce the nucleophilic substitution and thereby leading to amide bond formation [12].

3.4. Structural analysis of FG films

The diffraction bands of FG films upon exposure to UV irradiation and CD addition are illustrated in Fig. 2c. The diffraction patterns of FG/CD composite films did not show any distinct peak resulting from CD, most likely due to the low CD content and/or good dispersibility of CD within FG films. The XRD patterns of FG films showed a sharp peak at about 7.5° of 2θ due to the triple helix crystalline structure, while a broad peak at about 20° of 2θ was ascribed to the random coil conformation of gelatin [44]. Both the diffraction peaks were attributed to the partially crystalline nature of the gelatin films [45].

The crystallinity of films, as depicted in Table 1, did not change significantly upon UV exposure. In contrast, the addition of CD decreased the crystallinity of FG films considerably. Particularly, FG films became more amorphous in nature upon CD addition. The formation of crosslinks between CD and protein might hinder the reassembling of the triple helix structure of gelatin and thereby reduce the intermolecular interaction among protein chains leading to gradual loss of crystallinity during the film formation [11,46]. These findings are consistent with previous studies, where crystallinity loss of the gelatin composite films was attributed to the slower renaturation process of the triple helix structure of gelatin when graphene oxide with oxygen-containing surface functional groups was incorporated into the gelatin matrix [45,47]. Slower renaturation might lead to the enhanced stiffness of the gelatin chains as supported by the mechanical properties of FG films upon CD addition in the later discussion.

3.5. Thermal characterization of FG films

Thermal stability of the films after crosslinking can be evaluated by monitoring the glass transition temperature (Tg) with DSC [41]. DSC thermograms show the Tg of blank FG film at 72.88 °C before UV exposure and CD addition in Fig. 2d. After UV exposure, the Tg of FG-UV film increased to 78.28 °C. Benbettaieb et al. found similar results in the case of FG films crosslinked with electron-beam (EB) irradiation [48]. Both UV and EB irradiations as physical crosslinkers produce free

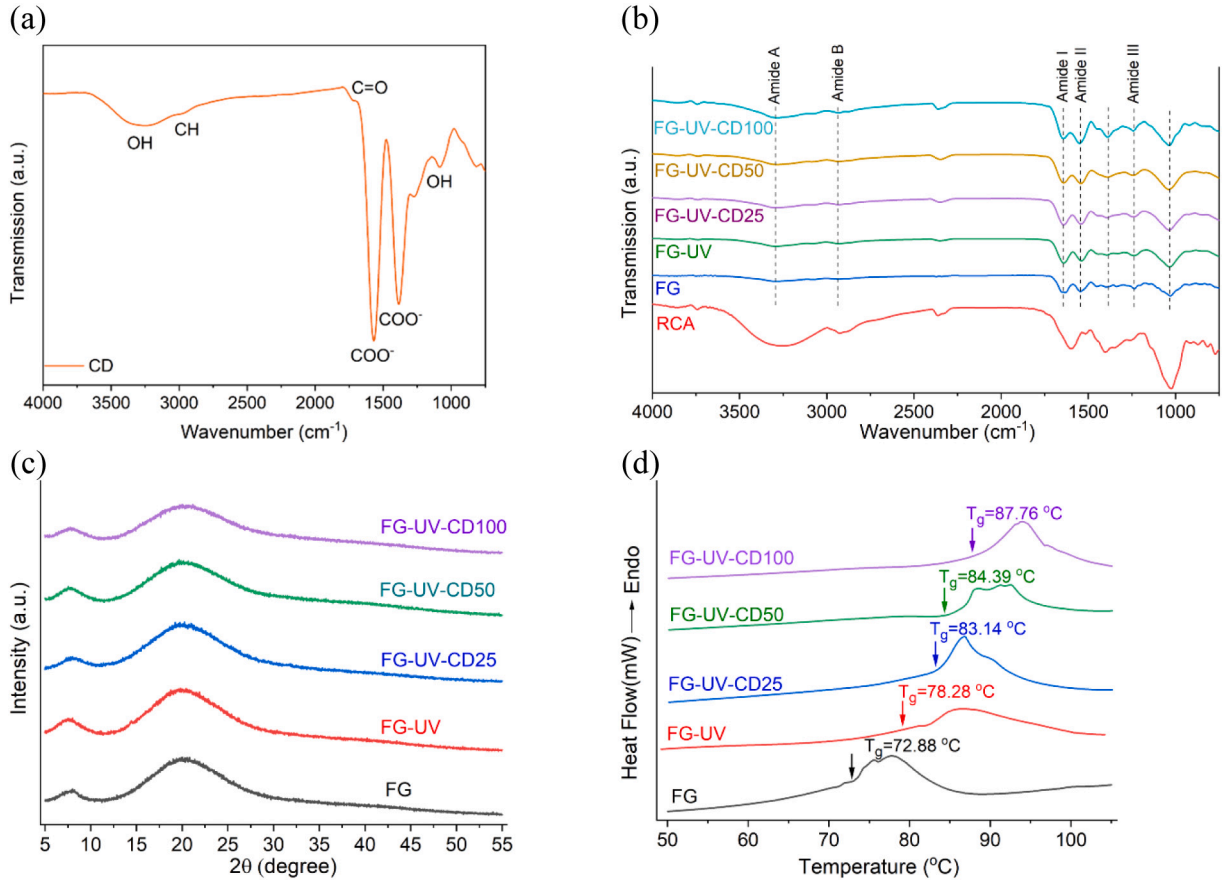

Fig. 2. FTIR spectra of (a) CD and (b) RCA and FG films (c) XRD patterns of FG films (d) DSC thermograms of FG films.

Table 1
Percent relative crystallinity of FG films.*

Sample	% relative crystallinity
FG	14.55 ± 0.26^{ab}
FG-UV	14.84 ± 0.12^{a}
FG-UV-CD25	14.07 ± 0.14^{abc}
FG-UV-CD50	13.65 ± 0.46^{bc}
FG-UV-CD100	13.09 ± 0.06^{c}

* Different superscript letters in the same column indicate significant differences ($p < 0.05$).

radicals predominately from the aromatic acyl residues of gelatin and water, respectively. Free radical generation induced by irradiation increases the crosslinking density, usually with an increase of Tg due to the reduced mobility of gelatin chain segments [48]. After addition of CD as the chemical crosslinker, the Tg increased further from 78.28 °C in FG-UV film to 83.14 °C in FG-UV-CD25 film, to 84.39 °C in FG-UV-CD50 and to 87.76 °C in FG-UV-CD100 film. This change might be ascribed to the effect of the crosslinking agent on the gelatin molecules. Guo et al. reported that gallic-acid crosslinked gelatin films showed higher Tg [49]. The increasing trend of the Tg values was attributed to covalently crosslinked network formation induced by a chemical crosslinker. Consistently, the results in this study indicate an increasing trend of Tg upon the addition of more CDs, which could impede the chain mobility of gelatin as a result of amide and hydrogen bonding between CD and FG. Overall, the DSC results support the conclusions derived from the XRD analysis.

3.6. Water solubility, barrier and mechanical properties of FG films

The WS values of the films are given in Table 2. WS shows the water tolerance of the films. FG control films indicated the lowest water resistance at 82% solubility among the tested films. Similar WS values were observed for gelatin from cold-water fish skin in the literature [50]. UV irradiation lowered the solubility of FG-UV films significantly compared to that of untreated FG films. This would be attributed to an increase in the crosslinking density of FG. Under UV irradiation, radicals generated at the aromatic residues of gelatin amino acids might initiate the intermolecular crosslinking of gelatin molecules [10]. Further, WS of films decreased significantly with the addition of CDs at different concentrations, as expected. The solubility of FG films went down to 38% with the addition of CD at 100 mg/l. Earlier, the presence of different crosslinkers, mostly simple sugars, in the precursor solutions has been demonstrated to lower the WS of the resulting FG films [51,52]. Similarly, multiple crosslinking agents in this study (i.e., CD and UV irradiation) might enhance the intermolecular interactions and, in turn, lower the solubility more rapidly by increasing the number of junction zones in the gelatin matrix.

Tensile (TS) and elongation at break (EAB) of FG films at different CD concentrations and with/without UV irradiation are shown in Table 2. TS is an indicator of film strength and, thereby one of the key parameters in determining the mechanical properties of food packaging films. There was a significant increase in the TS of FG films after UV exposure. Previous studies also reported an improvement in the TS of FG films upon UV irradiation treatment [7,10]. An increase in TS of protein-based films suggests that some UV induced crosslinking occurred [53]. Further, the addition of CDs improved the TS of FG films compared to neat control films due to enhanced intermolecular interactions. In particular, amide and hydrogen bonds were formed between the surface functional groups

Table 2
The effect of UV exposure and the addition of CDs at different concentrations on water solubility, mechanical and barrier properties of the fish gelatin films.*

Film type	WS (%)	Tensile (MPa)	EAB (%)	Thickness (mm)	WVP (x10^{-10} g m^{-1} s^{-1} Pa^{-1})
FG (untreated)	82.29 ± 3.37^{a}	22.64 ± 0.60^{a}	223.16 ± 20.16^{a}	0.19 ± 0.01^{a}	7.11 ± 1.10^{a}
FG-UV	63.52 ± 3.39^{b}	30.69 ± 0.57^{b}	117.75 ± 4.21^{b}	0.17 ± 0.02^{a}	5.33 ± 0.21^{ab}
FG-UV-CD25	56.25 ± 1.59^{bc}	34.48 ± 1.12^{c}	136.78 ± 5.76^{b}	0.16 ± 0.01^{a}	4.57 ± 0.29^{bc}
FG-UV-CD50	49.77 ± 2.80^{c}	34.85 ± 1.47^{c}	124.22 ± 8.11^{b}	0.17 ± 0.01^{a}	4.53 ± 0.04^{bc}
FG-UV-CD100	38.76 ± 2.18^{d}	36.94 ± 0.42^{c}	120.66 ± 1.87^{b}	0.20 ± 0.01^{a}	2.97 ± 0.07^{c}

* Different superscript letters in the same column indicate significant differences ($p < 0.05$).

of CDs (including hydroxyl and carboxyl) and FG, as evidenced in the surface analysis of ATR-FTIR. The obtained results are in good agreement with the literature, where significant improvements in the TS of soy protein isolate and gelatin/carrageenan composite films were observed upon incorporating CDs into film matrices [42,54].

The flexibility of the films after exposure to physical and chemical crosslinking agents was monitored through the change in EAB. EAB of FG films showed an opposite trend compared to TS and decreased significantly after UV exposure. This opposite relationship between TS and EAB has been reported for UV-treated films earlier [4]. Similarly, the addition of CDs under UV treatment led to a significant reduction in EAB compared to that of neat control FG films while EAB values of FG-UV films did not change significantly at different CD concentrations. There was a decreasing trend in EAB as the amount of CDs increased in the matrix. This restriction in the matrix motion might be attributed to the enhancement of the interaction between CD and FG upon addition of more CDs. Similar trends in the mechanical properties were observed when CD was incorporated into soy protein isolate film [37,42]. Overall, the enhanced mechanical properties of CD incorporated FG films might be explained by the excellent interactions between CDs and FG through amide and hydrogen bond formations under UV irradiation, which ultimately results in good dispersion of CDs in the FG matrix.

WVP of the film defines the water vapor barrier properties of the film. A low WVP value is vital for packaging films to restrict the transfer of water vapor from one side of the film to another. FG films might suffer from characteristic thickness effect, which shows a positive correlation between thickness and permeability properties of hydrophilic film systems due to the water vapor pressure variations at the film underside during testing [28]. In order to overrule this effect, it is crucial to compare the film thicknesses. In the current study, the addition of CD and UV exposure had little or no effect on film thickness among the tested films ($p < 0.05$). The WVP of FG films before and after UV irradiation is given in Table 2. There was a decreasing trend, but WVP values were not significantly affected by UV treatment among the control samples. Reportedly, a slight insignificant decrease in WVP values was also observed for different protein-based films after UV treatment [53]. WVP decreased significantly as CDs concentration increased in FG matrix under UV irradiation compared to untreated FG films ($p < 0.05$). Extensive crosslinking is required to observe a significant reduction in the WVP of the highly hydrophilic protein-based films. Thus, this reduction might be ascribed to hydrogen bond formation between CDs and FG matrix, which might make the hydrophilic sites less available for water vapor attachment and, thereby permeation [55]. In addition to hydrogen bonding, covalent conjugation of CDs to the FG matrix might increase the tortuosity of the pathway for the diffusion of water vapor as a result of highly crosslinked network formation [42].

3.7. Microstructural characterization of FG films

The cross sectional morphologies of the FG films were analyzed by FESEM. The unmodified FG film showed a smooth and dense structure of the FG matrix in general, as shown in Fig. 3a. This homogeneous and compact structure would be ascribed to a low physical interaction degree in untreated FG films, which led to the lowest TS (22.64 ± 0.60 MPa). UV treatment did not cause any morphologically obvious change in FG-UV samples. After CD addition, cross sectional views of the films reveal rough and crack surfaces. This morphological change intensified with the increase of CD concentration in the FG matrix [43]. This visible evidence is also supported by the crystalline phase change of the FG matrix as discussed in XRD and by improved mechanical properties of FG films upon CD addition. In this context, observed uneven and wavy cross sections in FESEM images might be considered as direct evidence for enhanced crosslinking after CD addition.

3.8. Colorimetric response to ammonia vapor

During spoilage of the protein-rich food, by its nature meat, volatile basic amines including ammonia, trimethylamine and dimethylamine are generated as a result of bacterial and enzymatic activities [6]. Ammonia with the lowest boiling point among TVB-N compounds is commonly used as a spoilage indicator for protein-rich food. In this sense, FG films are exposed to the ammonia gas generated from the aqueous solution of 0.8 M ammonia for 16 min at 23 °C. The initial maximum absorption peak was monitored at 530 nm for all films which was red-shifted from the absorption peak of the RCA solution at 520 nm. A similar red shift on the absorption spectra was also observed in roselle anthocyanins containing starch and polyvinyl alcohol based films [56]. The absorption peak at 530 nm decreased while another peak at 605 nm appeared and gradually increased with the concentration of ammonia vapor. The absorbance ratio of the films at 605 nm versus 530 nm (A605/A530) indicated the green color intensity relative to the red color intensity [57], which increased with time, as illustrated in Fig. 4. The slope of the curves represents the rate of color change from red to green and in turn, a higher slope shows a greater color variation [56]. The smallest slope values were obtained for control samples, namely FG and FG-UV (Fig. 4a). The highest color variation rate was obtained with FG-

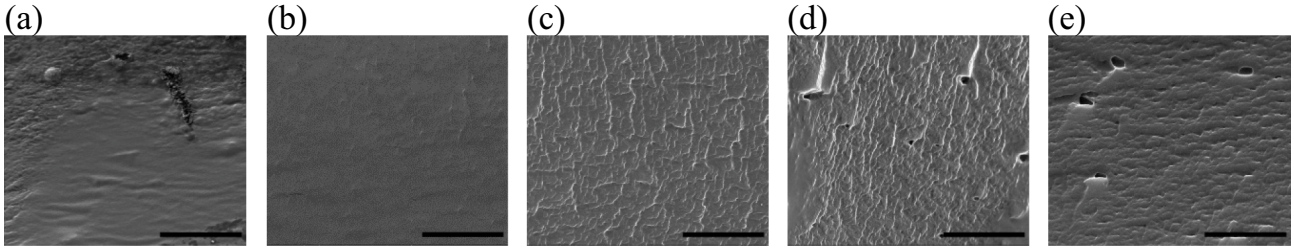

Fig. 3. FESEM images of (a) FG (b)FG-UV (c) FG-UV-CD25 |(d) FG-UV-CD50 (e) FG-UV-CD100. (Scale bar: 10 μm).

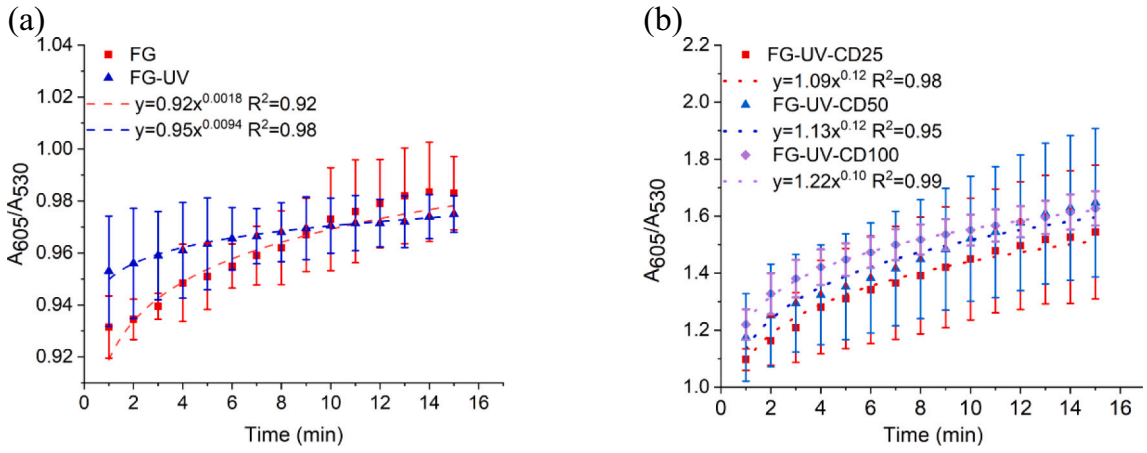

Fig. 4. The change of UV–Vis absorbance ratio (A605/A530) for (a) control FG films and (b) CD doped FG films when the films were exposed to 0.8 M ammonia solution at 23 °C for 16 min.

UV-CD100, followed by FG-UV-CD50 and then by FG-UV-CD25 (Fig. 4b). This result shows that the colorimetric film with the highest CD concentration is more sensitive to ammonia and, thereby TVB-N compounds. Ammonia interacts with carbonyl and hydroxyl groups of anthocyanins in the films and induces the color change. Besides, CDs appear light yellow in the acidic solution and gradually turn to yellowish orange in color as the pH increases. This color change can even be observed by naked eyes, as illustrated in Fig. S3. Similar pH dependencies in the color of CDs are observed earlier and associated with electronic transition shifts between π−π* and η−π* in nano domains by depleting or refilling their valence bands [58]. The apparent pH induced color evolution based on CDs might be the major reason behind the highest sensitivity of FG-UV-CD100 films against the TVB-N indicator, ammonia. Overall, FG-UV-CD100 film showing good mechanical properties with the lowest WVP and the highest color variation rate in response to TVB-N is chosen to investigate its potential use in smart food packaging applications.

We used the change in the a* and ΔE values of FG-UV-CD100 film to evaluate its performance as a colorimetric smart packaging label. For this purpose, the a* and ΔE values of FG-UV-CD100 film against different concentrations of volatile ammonia were determined and tabulated in Table 3 with the corresponding images of the films. The color of the films changed from red to green when exposed to a level of ammonia in a range of 0 to 120 mg/100 g. The a* value of the films decreased gradually and significantly starting from the ammonia concentration of 5 mg/100 g ($p < 0.05$). This result complies well with the observed color change as the positive values of a* indicates a greater red intensity while the negative values of a* show a greater tendency to green color. Correspondingly, the ΔE value of the films increased significantly in a concentration dependent manner up to ammonia concentration of 120 mg/100 g ($p < 0.05$). When exposed to different ammonia concentrations, ΔE values were all observed to be greater than 5, which shows that the color difference of the films is visually perceivable compared to its original color reference [59]. The above results showed the good performance of FG-UV-CD100 film on indicating the variation of surroundings volatile ammonia concentration. Thus, food sample trials were performed with FG-UVCD100 films in the following section.

3.9. Application of smart label in chicken spoilage trials

Total viable count (TVC) is widely considered a good indication of

Table 3
The color change of FG-CD-100 film against varying ammonia gas concentration.*

Ammonia gas concentration	Film response images	ΔE	a*
0 mg/ 100 g (Reference)		0	28.50±1.29[a]
5 mg/100 g		4.33±0.46[a]	27.25±1.26[a]
10 mg/100 g		12.16±0.36[b]	20.00±0.82[c]
20 mg /100 g		22.57±4.21[c]	9.25±4.11[d]
30 mg/100g		34.43±0.55[d]	-4.75±1.26[e]
60 mg/100 g		39.06±0.29[e]	-9.50±1.29[f]
90 mg/100 g		46.34±0.76[f]	-15.25±0.96[g]
120 mg/ 100 g		45.37±0.454[f]	-14.75±0.50[g]

* Different supercript letter in the same column indicate significant differences ($p<0.05$).

food microbial quality. For this reason, skinless chicken breast samples were examined for levels of total viable aerobic bacteria. As illustrated in Fig. 5a, TVC values of chicken samples increased significantly during the storage at 4 °C ($p < 0.05$). 6.7 log cfu/g is accepted as the maximum limit for raw chicken according to the Turkish Standard (TS 24019:2014) and European legislation (EC Regulation 1441/2007, 2007). This critical level was reached and exceeded after 7 days of storage at 4 °C. This result was comparable to the shelf-life studies of chicken performed by Kuswandi et al. [30], which also observed the onset of broiler chicken cut spoilage after 7 days at 4 °C [30]. Off-flavor formation of the spoiled protein-rich food is generally attributed to TVB-N generation as a result of microbial and enzymatic activities. Thus, the TVB-N level was used in this study as the chemical indicator to monitor the chicken freshness in real-time with FG-UV-CD100 films. Based on the results of ammonia sensitivity, it was expected to observe a colorimetric response with FG-UVCD100 films to TVB-N upon the onset of spoilage. The a* values and ΔE values with color transition of the films are given relative to the change in TVB-N levels of chicken samples during 9 days storage at 4 °C in Fig. 5a and b, respectively. The color of the films remained almost the same as brick red for the first 5 days. Similarly, the a* and ΔE values of the films did not change significantly during the same period of the time. The critical TVB-N level of 30 mg N/100 g is set for chicken carcasses by the Turkish Standard (TS2409:2014). The values of TVB-N were lower than this rejection limit within the first 6 days. At the day 7,the TVB-N level reached 30.2 ± 1.98 mg N/100 g indicating the spoilage of chicken samples. Correspondingly, the visually distinctive color change was observed after 6 days of storage. The color turned to green completely on the day 7 with a significant decrease in the a* value of the films. On the other hand, this color transition from red to green led to a significant increase in the ΔE value. TVB-N levels of chicken breast samples increased continuously similar to the microbial load during 9 days storage at 4 °C in Fig. 5c. Both maximum acceptable level of TVC and the critical TVB-N value was reached and exceeded after 7 days of storage. This result agrees with the findings of Kuswandi et al. [30], where the critical TVB-N level was also observed after 7 days for the chicken samples stored at 4 °C [30]. Overall, the color of FG-UV-CD100 film, thereby its a* and ΔE values, changed significantly in accordance with the variation of TVB-N and TVC levels at the onset of the spoilage.

3.10. Colorimetric analysis and calibration curve extraction

For the colorimetric analysis of food spoilage, the calibration curve with the highest R^2 value needs to be utilized. In this regard, 33 calibration curves were derived using the extracted features (Section 2.4). Among them, a* kurtosis was selected due to its R^2 value as illustrated in Fig. 5d. To obtain the calibration curve, images were captured when the films were exposed to different ammonia concentrations, including 5 mg/100 g, 10 mg/100 g, 20 mg/100 g, 30 mg/100 g, 60 mg/100 g, 90 mg/100 g, 120 mg/100 g.

The highest value of R^2 was obtained with the a* kurtosis feature as 0.99. The equation of a* kurtosis was derived to embed into our custom-designed Android application *SmartFood* given in Fig. 6, where a demonstration was shown for the two different images selected from the gallery. The images were cropped separately with the adjustable box to obtain the ROI (Fig. 6b-c-e-f). Next, the a* kurtosis feature of the ROI was calculated to find the corresponding concentration value using the calibration curve for these two images (Fig. 6c and f). The estimated concentrations of ROIs were 4.28 mg/100 g and 41.82 mg/100 g, as shown in Fig. 6d and g, respectively. Moreover, our application informs the user with various stickers based on the test result. If the food is consumable, the "Bon Appetit" text under a happy-face sticker is

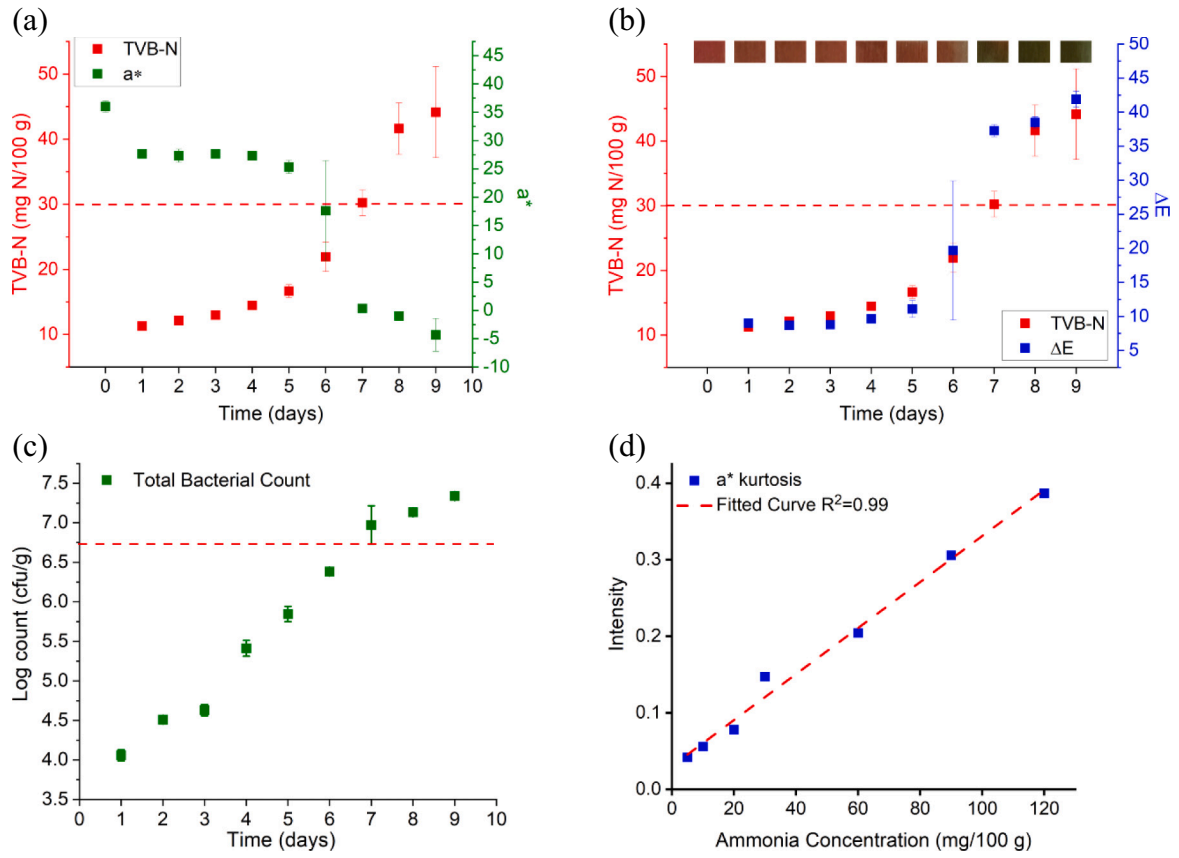

Fig. 5. Changes in TVB-N (a) with a* value and (b) with ΔE value and changes in (c) TVC during 9 days storage of skinless chicken at 4 °C. (d) The calibration curve with a* kurtosis feature.

Fig. 6. The steps for colorimetric food spoilage monitoring in *SmartFood* are as follows. The homepage of *SmartFood* is given in (a). The user can select an image from the gallery or capture a new image using the smartphone camera and crop the image using an adjustable crop box as in (b) and (e). Cropped patches are given in (c) and (f). The application is tested with the consumable food (chicken) in (d), and the inconsumable one in (g).

displayed on the screen (Fig. 6d). Otherwise, it shows a sad-face sticker with "Inconsumable" text (Fig. 6g).

4. Conclusion

In the present study, we developed colorimetric fish gelatin films based on red cabbage anthocyanins extract using UV irradiation as a physical crosslinker and the CD as a chemical crosslinker to monitor the food spoilage based on a color change. The effect of CD addition was more prominent compared to that of UV exposure on the tested properties of the FG films. The FTIR spectra of the colorimetric films showed that CDs were successfully incorporated into the FG matrix through the amide bond formation. In this sense, the crystallinity of the films was reduced as an indicator of crosslinking between CD and amino acid residues of FG while the water tolerance, mechanical, thermal and barrier properties of the FG films were improved. Among the tested films, FG-UV-CD100 films showed the best sensitivity to ammonia. Later, the color response of FG-UV-CD100 films was found to correlate well with microbial growth and TVB-N release in skinless chicken breast samples, therefore denoting its potential for applications in real-time monitoring of spoilage. In this regard, a custom-designed smartphone application (*SmartFood*) capable of image processing was developed for quantitative analysis of food spoilage. The embedded analyzing tool in the *SmartFood* monitors the level of spoilage and informs the user about the current freshness status of the food. The proposed platform has a great potential to provide real-time information on food quality/freshness, leading to the protection of consumers against potential foodborne illness and the prevention of global food waste.

CRediT authorship contribution statement

Munevver Beyza Kilic: Methodology, Investigation, Writing.
Vakkas Dogan: Software, Investigation, Writing.
Volkan Kilic: Conceptualization, Supervision, Review and Editing.
Leyla Nesrin Kahyaoglu: Conceptualization, Supervision, Review and Editing, Financial Acquisition.

Acknowledgements

This research was supported by the Scientific and Technological Research Council of Turkey (TUBITAK) (No. 119O864).

Appendix A. Supplementary data

Supplementary data to this article can be found online at https://doi.org/10.1016/j.ijbiomac.2022.04.119.

References

[1] N.L.W. Wilson, B.J. Rickard, R. Saputo, S.-T. Ho, Food waste: the role of date labels, package size, and product category, Food Qual. Prefer. 55 (2017) 35–44.
[2] Y. Chen, G. Fu, Y. Zilberman, W. Ruan, S.K. Ameri, Y.S. Zhang, E. Miller, S. R. Sonkusale, Low cost smart phone diagnostics for food using paper-based colorimetric sensor arrays, Food Control 82 (2017) 227–232.
[3] M. Sohail, D.-W. Sun, Z. Zhu, Recent developments in intelligent packaging for enhancing food quality and safety, Crit. Rev. Food Sci. Nutr. 58 (2018) 2650–2662.
[4] D. Dainelli, N. Gontard, D. Spyropoulos, E. Zondervan-van den Beuken, P. Tobback, Active and intelligent food packaging: legal aspects and safety concerns, Trends Food Sci. Technol. 19 (2008). S103-S112.

[5] P. Müller, M. Schmid, Intelligent packaging in the food sector: a brief overview, Foods 8 (2019).
[6] M. Moradi, H. Tajik, H. Almasi, M. Forough, P. Ezati, A novel pH sensing indicator based on bacterial cellulose nanofibers and black carrot anthocyanins for monitoring fish freshness, Carbohydr. Polym. 222 (2019), 115030.
[7] C.G. Otoni, R.J. Avena-Bustillos, B.S. Chiou, C. Bilbao-Sainz, P.J. Bechtel, T. H. McHugh, Ultraviolet-B radiation induced crosslinking improves physical properties of cold- and warm-water fish gelatin gels and films, J. Food Sci. 77 (2012). E215-E223.
[8] A.A. Karim, R. Bhat, Fish gelatin: properties, challenges, and prospects as an alternative to mammalian gelatins, Food Hydrocoll. 23 (2009) 563–576.
[9] R.J. Avena-Bustillos, C.W. Olsen, D.A. Olson, B. Chiou, E. Yee, P.J. Bechtel, T. H. McHugh, Water vapor permeability of mammalian and fish gelatin films, J. Food Sci. 71 (2006). E202-E207.
[10] R. Bhat, A.A. Karim, Towards producing novel fish gelatin films by combination treatments of ultraviolet radiation and sugars (ribose and lactose) as cross-linking agents, J. Food Sci. Technol. 51 (2014) 1326–1333.
[11] A. Etxabide, J. Uranga, P. Guerrero, K. de la Caba, Improvement of barrier properties of fish gelatin films promoted by gelatin glycation with lactose at high temperatures, LWT 63 (2015) 315–321.
[12] J. Uranga, I. Leceta, A. Etxabide, P. Guerrero, K. de la Caba, Crosslinking of fish gelatins to develop sustainable films with enhanced properties, Eur. Polym. J. 78 (2016) 82–90.
[13] M. Araghi, Z. Moslehi, A.M. Nafchi, A. Mostahsan, N. Salamat, A.D. Garmakhany, Cold water fish gelatin modification by a natural phenolic cross-linker (ferulic acid and caffeic acid), Food Sci. Nutr. 3 (2015) 370–375.
[14] M. Rezaee, G. Askari, Z. EmamDjomeh, M. Salami, UV-irradiated gelatin-chitosan bio-based composite film, physiochemical features and release properties for packaging applications, Int. J. Biol. Macromol. 147 (2020) 990–996.
[15] R. Bhat, A.A. Karim, Ultraviolet irradiation improves gel strength of fish gelatin, Food Chem. 113 (2009) 1160–1164.
[16] N. Dhenadhayalan, K.-C. Lin, R. Suresh, P. Ramamurthy, Unravelling the multiple emissive states in citric-acid-derived carbon dots, J. Phys. Chem. C 120 (2016) 1252–1261.
[17] Y. Yu, C. Li, C. Chen, H. Huang, C. Liang, Y. Lou, X.-B. Chen, Z. Shi, S. Feng, Saccharomyces-derived carbon dots for biosensing pH and vitamin B 12, Talanta 195 (2019) 117–126.
[18] A.Y. Mutlu, V. Kılıç, Machine learning based smartphone spectrometer for harmful dyes detection in water, in: 26th Signal Processing and Communications Applications Conference (SIU), IEEE, 2018, pp. 1–4.
[19] Ö.B. Mercan, V. Kılıç, Fuzzy classifier based colorimetric quantification using a smartphone, in: International Conference on Intelligent and Fuzzy Systems, Springer, 2020, pp. 1276–1283.
[20] V. Doğan, E. Yüzer, V. Kilic, M. Şen, Non-enzymatic colorimetric detection of hydrogen peroxide using a μpad coupled with a machine learning-based smartphone app, Analyst (2021) 7336–7344.
[21] T. Golcez, V. Kilic, M. Sen, A portable smartphone-based platform with an offline image processing tool for rapid paper-based colorimetric detection of glucose in artificial saliva, Anal. Sci. 37 (2021) 561–568.
[22] V. Kılıç, O.B. Mercan, M. Tetik, O. Kap, N. Horzum, Non-enzymatic colorimetric glucose detection based on Au/Ag nanoparticles using smartphone and machine learning, Anal. Sci. 38 (2022) 347–358.
[23] Ö. Kap, V. Kılıç, J.G. Hardy, N. Horzum, Smartphone-based colorimetric detection systems for glucose monitoring in the diagnosis and management of diabetes, Analyst 146 (2021) 2784–2806.
[24] T. Gölcez, V. Kılıç, M. Şen, Integration of a smartphone application with a 1/4pad for rapid colorimetric detection of glucose, in: 2019 Medical Technologies Congress (TIPTEKNO), IEEE, 2019, pp. 1–4.
[25] V. Kılıç, M. Şen, Smartphone-based colorimetric analysis for the detection of h 2 o 2 using a 1/4pad, in: 2019 Medical Technologies Congress (TIPTEKNO), IEEE, 2019, pp. 1–4.
[26] J. Chandrasekhar, M.C. Madhusudhan, K.S. Raghavarao, Extraction of anthocyanins from red cabbage and purification using adsorption, Food Bioprod. Process. 90 (2012) 615–623.
[27] T. Fuleki, F.J. Francis, Quantitative methods for anthocyanins, J. Food Sci. 33 (1968) 78–83.
[28] T.H. Mchugh, R. Avena-Bustillos, J.M. Krochta, Hydrophilic edible films: modified procedure for water vapor permeability and explanation of thickness effects, J. Food Sci. 58 (1993) 899–903.
[29] N. Gontard, C. Duchez, J.-L. Cuq, S. Guilbert, Edible composite films of wheat gluten and lipids: water vapour permeability and other physical properties, Int. J. Food Sci. Technol. 29 (1994) 39–50.
[30] B. Kuswandi, Jayus, A. Restyana, A. Abdullah, L.Y. Heng, M. Ahmad, A novel colorimetric food package label for fish spoilage based on polyaniline film, Food Control 25 (2012) 184–189.
[31] Z. Ma, P. Chen, W. Cheng, K. Yan, L. Pan, Y. Shi, G. Yu, Highly sensitive, printable nanostructured conductive polymer wireless sensor for food spoilage detection, Nano Lett. 18 (2018) 4570–4575. PMID: 29947228.
[32] E. Yildiz, G. Sumnu, L.N. Kahyaoglu, Monitoring freshness of chicken breast by using natural halochromic curcumin loaded chitosan/PEO nanofibers as an intelligent package, Int. J. Biol. Macromol. 170 (2021) 437–446.
[33] C. Rukchon, A. Nopwinyuwong, S. Trevanich, T. Jinkarn, P. Suppakul, Development of a food spoilage indicator for monitoring freshness of skinless chicken breast, Talanta 130 (2014) 547–554.
[34] T. Liang, G. Sun, L. Cao, J. Li, L. Wang, A pH and NH3 sensing intelligent film based on Artemisia sphaerocephala krasch. Gum and red cabbage anthocyanins anchored by carboxymethyl cellulose sodium added as a host complex, Food Hydrocoll. 87 (2019) 858–868.
[35] P.A.V. Freitas, T.V. de Oliveira, R.R.A. Silva, A.R. Fialho e Moraes, A.C.D.S. Pires, R.R.A. Soares, N.S. Junior, N.F.F. Soares, Effect of pH on the intelligent film-forming solutions produced with red cabbage extract and hydroxypropylmethylcellulose, Food Packag. Shelf Life 26 (2020), 100604.
[36] M. Amjad, M. Iqbal, A. Faisal, A.M. Junjua, I. Hussain, S.Z. Hussain, H.A. Ghramh, K.A. Khan, H.A. Janjua, Hydrothermal synthesis of carbon nanodots from bovine gelatin and PHM3 microalgae strain for anticancer and bioimaging applications, Nanoscale Adv. 1 (2019) 2924–2936.
[37] S. Rani, K.D. Kumar, S. Mandal, R. Kumar, Functionalized carbon dot nanoparticles reinforced soy protein isolate biopolymeric film, J. Polym. Res. 27 (2020) 312.
[38] H. Xu, X. Yang, G. Li, C. Zhao, X. Liao, Green synthesis of fluorescent carbon dots for selective detection of tartrazine in food samples, J. Agric. Food Chem. 63 (2015) 6707–6714.
[39] R. Ramamoorthy, N. Radha, G. Maheswari, S. Anandan, S. Manoharan, R. Victor Williams, Betalain and anthocyanin dye-sensitized solar cells, J. Appl. Electrochem. 46 (2016) 929–941.
[40] V.A.J. Pereira, I.N. Queiroz de Arruda, R. Stefani, Active chitosan/ PVA films with anthocyanins from brassica oleraceae (Red Cabbage) as time-temperature indicators for application in intelligent food packaging, Food Hydrocoll. 43 (2015) 180–188.
[41] K. Nilsuwan, S. Benjakul, T. Prodpran, Properties and antioxidative activity of fish gelatin-based film incorporated with epigallocatechin gallate, Food Hydrocoll. 80 (2018) 212–221.
[42] Y. Li, H. Chen, Y. Dong, K. Li, L. Li, J. Li, Carbon nanoparticles/soy protein isolate bio-films with excellent mechanical and water barrier properties, Ind. Crop. Prod. 82 (2016) 133–140.
[43] S.K. Bhattacharyya, M. Dule, R. Paul, J. Dash, M. Anas, T.K. Mandal, P. Das, N. C. Das, S. Banerjee, Carbon dot cross-linked gelatin nanocomposite hydrogel for ph-sensing and ph-responsive drug delivery, ACS Biomater Sci. Eng. 6 (2020) 5662–5674.
[44] A. Bigi, S. Panzavolta, K. Rubini, Relationship between triple-helix content and mechanical properties of gelatin films, Biomaterials 25 (2004) 5675–5680.
[45] A.Nor Adilah, C.Gun Hean, Z.A.Nur Hanani, Incorporation of graphene oxide to enhance fish gelatin as bio-packaging material, Food Packag. Shelf Life 28 (2021), 100679.
[46] J. Guo, L. Ge, X. Li, C. Mu, D. Li, Periodate oxidation of xanthan gum and its crosslinking effects on gelatin-based edible films, Food Hydrocoll. 39 (2014) 243–250.
[47] C. Wan, M. Frydrych, B. Chen, Strong and bioactive gelatin–graphene oxide nanocomposites, Soft Matter 7 (2011) 6159–6166.
[48] N. BenBettaieb, T. Karbowiak, C.-H. Brachais, F. Debeaufort, Impact of electron beam irradiation on fish gelatin film properties, Food Chem. 195 (2016) 11–18.
[49] L. Guo, T. Qiang, Y. Ma, L. Ren, C. Zhu, Biodegradable anti-ultraviolet film from modified gallic acid cross-linked gelatin, ACS Sustain. Chem. Eng. 9 (2021) 8393–8401.
[50] R. Jeya Shakila, E. Jeevithan, A. Varatharajakumar, G. Jeyasekaran, D. Sukumar, Comparison of the properties of multi-composite fish gelatin films with that of mammalian gelatin films, Food Chem. 135 (2012) 2260–2267.
[51] P. Hazaveh, A. MohammadiNafchi, H. Abbaspour, The effects of sugars on moisture sorption isotherm and functional properties of cold water fish gelatin films, Int. J. Biol. Macromol. 79 (2015) 370–376.
[52] H. Kchaou, N. BenBettaieb, M. Jridi, O. Abdelhedi, T. Karbowiak, C.-H. Brachais, M.-L. Léonard, F. Debeaufort, M. Nasri, Enhancement of structural, functional and antioxidant properties of fish gelatin films using maillard reactions, Food Hydrocoll. 83 (2018) 326–339.
[53] J.W. Rhim, A. Gennadios, D. Fu, C.L. Weller, M.A. Hanna, Properties of ultraviolet irradiated protein films, LWT Food Sci. Technol. 32 (1999) 129–133.
[54] S. Roy, P. Ezati, J.-W. Rhim, Gelatin/Carrageenan-based functional films with carbon dots from enoki mushroom for active food packaging applications, ACS Appl. Polym. Mater. 3 (2021) 6437–6445.
[55] J. Lee, K. Kim, Characteristics of soy protein isolate-montmorillonite composite films, J. Appl. Polym. Sci. 118 (2010) 2257–2263.
[56] X. Zhai, J. Shi, X. Zou, S. Wang, C. Jiang, J. Zhang, X. Huang, W. Zhang, M. Holmes, Novel colorimetric films based on starch/polyvinyl alcohol incorporated with roselle anthocyanins for fish freshness monitoring, Food Hydrocoll. 69 (2017) 308–317.
[57] I. Choi, J.Y. Lee, M. Lacroix, J. Han, Intelligent pH indicator film composed of agar/potato starch and anthocyanin extracts from purple sweet potato, Food Chem. 218 (2017) 122–128.
[58] X. Jia, J. Li, E. Wang, One-pot green synthesis of optically ph sensitive carbon dots with upconversion luminescence, Nanoscale 4 (2012) 5572–5575.
[59] S. Naghdi, M. Rezaei, M. Abdollahi, A starch-based pH-sensing and ammonia detector film containing betacyanin of paperflower for application in intelligent packaging of fish, Int. J. Biol. Macromol. 191 (2021) 161–170.